

APPLICATION OF URANS TURBULENCE CLOSURE MODELS TO COMPLEX FLOWS SUBJECTED TO ELECTROMAGNETIC AND OTHER BODY FORCES

D. R. Wilson, T. J. Craft and H. Iacovides

School of Mechanical, Aerospace and Civil Engineering
 The University of Manchester, Manchester, M13 9PL, UK
 dean.wilson@manchester.ac.uk

ABSTRACT

This paper considers the application of the Unsteady Reynolds Averaged Navier-Stokes (URANS) approach to two types of electromagnetically influenced turbulent flows. The first is a periodic 2D channel flow with an imposed wall normal magnetic field (Hartmann flow) and the second is that of Rayleigh-Bénard convection with a vertical magnetic field imposed. The turbulence is represented by a low- Re $k - \epsilon$ model which is tested with and without electromagnetic modifications proposed by Kenjereš & Hanjalić (2000). The results show the modifications lead to a dramatic reorganisation of the coherent structures in Rayleigh-Bénard convection as the magnetic field strength is increased, but over-predict the damping of the turbulent shear stress in a simple channel flow.

INTRODUCTION

Many flows of industrial and environmental significance are influenced by body forces of some kind. Those imposed by system rotation and electromagnetic fields, for example, are widely used as a means of processing and controlling metallic materials (Davidson, 1999) whilst those involved with heat transfer, such as buoyancy, are often required to be kept under control to ensure quality. In particular, a variety of novel uses for electromagnetic fields are emerging, most notably for targeted drug delivery, crystal growth and electromagnetic flow control. Since the optimization of such processes is increasingly dependant on the ability to model these flows accurately via CFD, the correct incorporation of these complex body forces is of clear importance.

For routine industrial computations, approaches which either fully or partially resolve the flow turbulence, such as Direct Numerical Simulation or Large Eddy Simulation (LES), are still computationally prohibitive despite the significant advancements in computational power during the last two decades. As such, and noting that most of the sub-scale models used in LES are derivatives of eddy-viscosity type Reynolds Averaged Navier-Stokes (RANS) models, it is relevant to address how various RANS models respond to the inclusion of the above force fields.

With electromagnetic fields, it is the relative motion between an electrically conducting fluid and a magnetic field which provides the Lorentz force. This acts in a plane perpendicular to the magnetic field and in opposition to the fluid velocity, resulting in a reduction of those components,

both mean and fluctuating, which are not aligned with the magnetic field. The effect of this preferential damping on the Reynolds stresses is generally an increased anisotropy; something that linear eddy-viscosity models (LEVM's) are unable to directly reproduce. A study by Hanjalić & Kenjereš (2000), however, showed that inclusion of indirect effects, through additional terms in the k and ϵ transport equations, could cause significant structural changes to the flow field.

This paper explores to what extent the LEVM approach can reproduce the reported effects of the different force fields on two test cases over a range of different flow field parameters. A simple 2D periodic channel flow is first examined, before several 3D convective flows are presented, in which both buoyancy and electromagnetic forces are influential. For the latter cases, the study reproduces and extends the results of Hanjalić & Kenjereš (2000) with the addition of stronger magnetic fields, and introduces new results, for the same magnetic field intensities, but at a much lower (and physically more relevant) Prandtl number.

GOVERNING EQUATIONS

The incompressible flow of an electrically conducting fluid subjected to both an imposed magnetic field and an imposed heat flux is governed by the equations of continuity, momentum and energy, together with Maxwell's equations of electromagnetism and Ohm's law for moving media. To account for buoyancy, the Boussinesq approximation is employed, and the buoyant force term in the momentum equations is then written as $F_i^b = -g_i\beta(\Theta - \Theta_0)$, where $\beta = 1/\Theta$ is the volume expansion coefficient and $\Theta_0 = (\Theta_{\text{hot}} - \Theta_{\text{cold}})/2$ is a reference temperature.

The coupling between the hydrodynamic and electromagnetic fields is through the Lorentz force $\mathbf{F}^L = \mathbf{J} \times \mathbf{B}$, where \mathbf{J} is the electric current and \mathbf{B} is the magnetic field. If the magnetic field associated with the induced currents is negligible (inductionless approximation) then the fluid flow has little effect on the magnetic field (i.e. the magnetic Reynolds number is $\ll 1$) and Maxwell's equations can be reduced, via Ohm's law and the conservation of current, to a single Poisson equation for the electric potential, ϕ ;

$$\nabla^2 \phi = \nabla \cdot (\mathbf{U} \times \mathbf{B}_0) \quad (1)$$

where \mathbf{B}_0 is the imposed magnetic field. The mean Lorentz

force can then be expressed as;

$$F_i^L = \sigma \left(-\varepsilon_{ijk} B_k \frac{\partial \phi}{\partial x_j} + U_k B_i B_k - U_i B_k^2 \right) \quad (2)$$

where σ is the electrical conductivity and ε_{ijk} is the Levi-Civita alternating tensor.

For the Reynolds and Rayleigh numbers considered in this study, it is computationally feasible to resolve the flow field right up to the walls, across the viscous sub-layer. The two-equation $k - \varepsilon$ model of Launder & Sharma (1974) has been employed, which includes relevant low- Re modifications. Exact expressions for the additional electromagnetic terms that should be present in the turbulence equations can be derived by including the fluctuating part of Lorentz force in the conventional derivation of the k and ε equations. For the k equation, this results in an unknown correlation between the fluctuating electric field and the fluctuating velocity, and terms involving the individual stress components. The term for the ε equation contains many more unknown correlations. Here we have used the additional modelled terms proposed by Kenjereš & Hanjalić (2000), referred to as the KH model hereafter, which are formed from the product of an inverse magnetic timescale and an exponential damping function which is dependant on the local turbulent time scale;

$$S_k^M = -\frac{\sigma}{\rho} B_0^2 k \exp \left(-C_L \frac{\sigma}{\rho} B_0^2 \frac{k}{\varepsilon} \right) \quad (3)$$

$$S_\varepsilon^M = -\frac{\sigma}{\rho} B_0^2 \varepsilon \exp \left(-C_L \frac{\sigma}{\rho} B_0^2 \frac{k}{\varepsilon} \right) \quad (4)$$

where the constant $C_L = 0.025$. For the turbulent heat flux, $\overline{u_i \theta}$, a simple eddy-diffusivity model has been employed.

NUMERICAL FORMULATION

All computations have been carried out using a version of the in-house 2D/3D finite-volume flow solver STREAM which has been extended to include the above modifications. The code utilizes structured non-orthogonal multi-block meshes with a collocated storage arrangement. The pressure is obtained through the SIMPLE algorithm, with Rhie & Chow interpolation to avoid checkerboarding. Convective terms in the momentum equations are treated with the bounded high-order UMIST scheme of Lien & Leschziner (1994) whilst those in the turbulence equations use the first order UPWIND scheme. For temporal discretization, the second-order accurate Crank-Nicolson scheme is used.

FULLY DEVELOPED HARTMANN FLOW

We first present results of the above models for the flow of an electrically conducting fluid through a 2D channel with electrically insulating walls and subjected to a wall normal magnetic field, termed Hartmann flow.

The strength of the magnetic field is quantified through the non-dimensional Hartmann number $Ha = B \delta \sqrt{\sigma/\mu}$, where δ is a characteristic length scale (the channel half-width). The flow is defined by the turbulent Reynolds number, $Re_\tau = \rho u_\tau \delta / \mu$, where u_τ is the friction velocity. Our

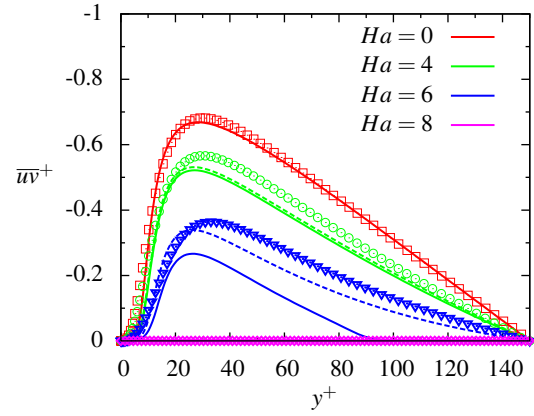


Figure 1. Turbulent shear stress $\overline{uv}^+ = \overline{uv}/u_\tau^2$ profiles for Hartmann flow at different Ha . Solid lines represent KH model, dashed lines represent standard low- Re $k - \varepsilon$ model, symbols are DNS data of Noguchi *et al.* (2004); $Re_\tau = 150$

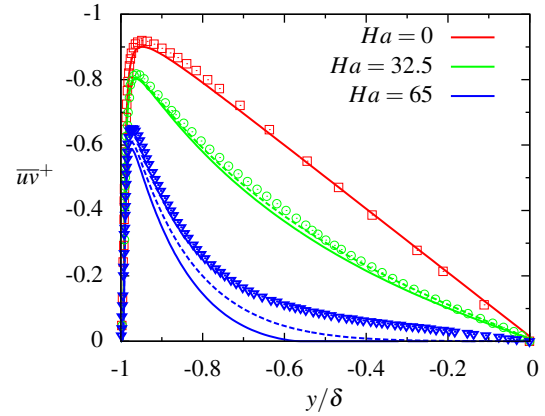


Figure 2. Turbulent shear stress $\overline{uv}^+ = \overline{uv}/u_\tau^2$ profiles for Hartmann flow at different Ha . Solid lines represent KH model, dashed lines represent standard low- Re $k - \varepsilon$ model, symbols are DNS data of Satake *et al.* (2006); $Re_\tau = 150$

interest lies only with the fully developed state, and thus periodic boundary conditions are employed in the stream-wise direction. Only a small (~ 10) number of control volumes are therefore required in this direction, which significantly reduces the computational cost. In the wall normal direction the grid is clustered towards the walls to facilitate solution resolution right up to the wall. A mesh was generated for each parameter combination to ensure that the near-wall node was well within the viscous sublayer, with the non-dimensional wall distance typically being less than unity. The parameter ranges considered are $Ha = 0, 4, 6, 8$ at a relatively low Reynolds number of $Re_\tau = 150$, for which comparisons are made against DNS data by Noguchi *et al.* (2004), and $Ha = 0, 32.5, 65$ at the higher Reynolds numbers of $Re_\tau = 1120, 1150, 1194$ respectively, for which comparisons are made against DNS data by Satake *et al.* (2006). The low- Re $k - \varepsilon$ model is tested both with and without the additional electromagnetic terms proposed by KH.

At low Re_τ , Figure 1 illustrates both forms of the model respond well to the increase in magnetic field strength. The reduction in shear stress is slightly over-predicted by both at low Ha , with the damping type terms in the KH model providing a small further reduction. At

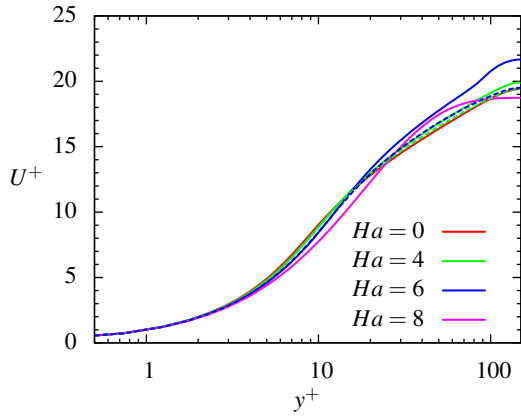


Figure 3. Velocity profiles for Hartmann flow at different Ha . Solid lines represent KH model, dashed lines represent standard low- Re $k - \epsilon$ model; $Re_\tau = 150$

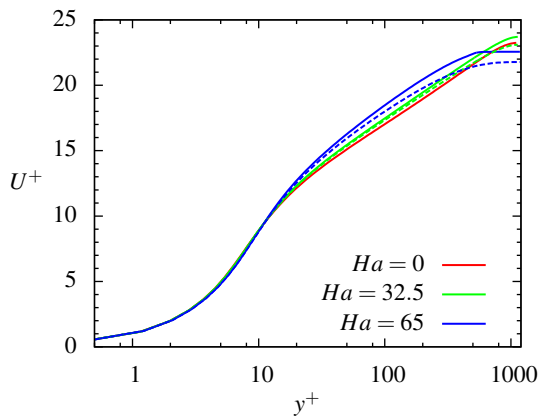


Figure 4. Velocity profiles for Hartmann flow at different Ha . Solid lines represent KH model, dashed lines represent standard low- Re $k - \epsilon$ model; $Re_\tau \approx 1150$

$Ha = 6$ however, the KH modification predicts an overly excessive reduction, with a much lower peak value and a laminar core region. At $Ha = 8$, both models correctly predict relaminarization of the flow in line with the DNS data. A similar trend is observed for the higher Re_τ cases (Figure 2), where at the highest Ha tested the predicted laminar core region extends further towards the wall than implied by the DNS. The peak values, however, are fairly well predicted.

The corresponding velocity profiles, Figures 3 and 4, show the action of the Lorentz force tends to cause the velocity profile to flatten, leading to a larger, more uniform, core region. The damping of the turbulence at $Ha = 6$ is clearly demonstrated by the departure of the profile from the log-law. For $Ha = 8$ the velocity profile is completely laminar and is in exact agreement with the corresponding analytical Hartmann solution. In the high- Re_τ flow at $Ha = 65$, the KH model predicts a completely flat profile in the core of the channel which corresponds to the laminar core.

To shed further light on the model performance, we note that the exact values of the S_k^M and S_ϵ^M terms are provided in the DNS by Noguchi *et al.* (2004), which reveals that both act as sinks across the entire channel width. Kenjereš & Hanjalić (2000) show that their modelled form underestimates S_ϵ^M throughout the region $0 < y^+ < 40$, which

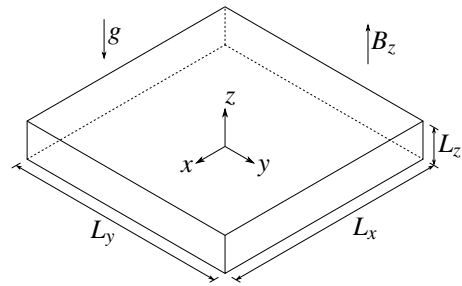


Figure 5. Geometry for Rayleigh-Bénard convection cases

corresponds to the location of the peak turbulence in Figure 1. Since in an LEVM $\overline{uv} \propto k^2/\epsilon$, an underestimated sink term for ϵ would cause an overprediction of ϵ and hence an underprediction of \overline{uv} . The discrepancy is not linear since the non-dimensional form of S_ϵ^M is proportional to Ha^2 .

RAYLEIGH-BÉNARD CONVECTION

We now present results of the KH model for cases of Rayleigh-Bénard convection between two infinite flat plates maintained at constant, but different, temperatures, with a magnetic field also applied in the vertical direction. Here, heat transfer to the fluid from the hot, lower surface causes buoyant plumes to rise whilst heat transfer from the fluid to the cooled, upper surface causes fluid to sink. The impingement of these plumes on the opposing surface causes horizontal motion and the end result is the establishment of a roll cell. With the addition of a magnetic field in the vertical direction the Lorentz force inhibits both mean and fluctuating horizontal motions, causing the roll cells to become thinner and more elongated.

The domain considered is an 8:8:1 aspect ratio rectangular cavity, shown in Figure 5. The Rayleigh number $Ra = g\beta\Delta\Theta L_z^3/\nu^2 = 10^7$, is well within the turbulent regime for the non-magnetic case, and the magnetic field strength is considered in the range $0 < Ha < 200$. For each magnetic field strength, two Prandtl numbers are considered $Pr = 0.71$ and $Pr = 0.01$. The mesh employed has a resolution of $N_x \times N_y \times N_z = 80 \times 80 \times 100$ with cells clustered towards the walls to ensure the validity of the low- Re modelling approach and the non-dimensional time step $\Delta t \sqrt{g\beta\Delta\Theta/L_z} = 0.02$. For the moderate Prandtl number, comparisons at $Ha = 0, 20$ and 100 are made with URANS results from Hanjalić & Kenjereš (2000) who used a low- Re three-equation $k - \epsilon - \overline{\theta}^2$ model with an algebraic expression for the turbulent heat fluxes.

As validation of the code, we first present comparisons of the long-term time averaged temperature profiles in the vertical plane with the DNS data of Wörner (1994). Computations were performed at $Ra = 6.3 \times 10^5$ and show excellent quantitative agreement, as seen in Figure 6. The profile exhibits a uniform core region flanked by thermal boundary layers which are characteristic of Rayleigh-Bénard convection.

Moderate Prandtl Number Cases

Figures 7 and 8 show the effect of the vertical magnetic field on the long-term time averaged temperature and modelled turbulent kinetic energy for the case with $Pr = 0.71$. A low magnetic field ($Ha = 20$) provides a slight, but no-

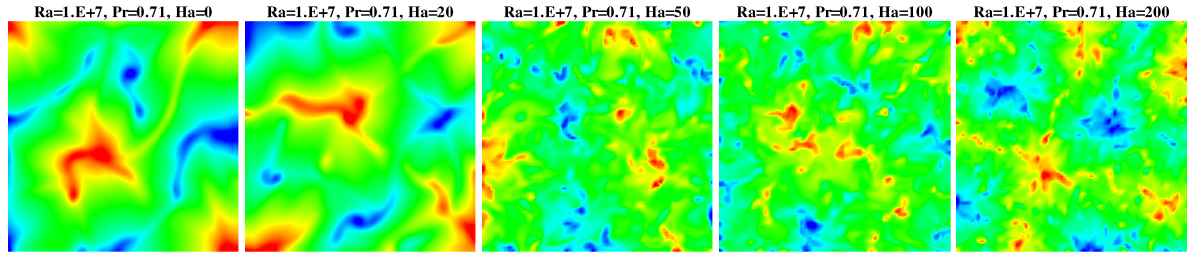


Figure 9. Snapshots showing contours of non-dimensional temperature ($0.3 < \Theta < 0.7$) in the central horizontal plane, $z/L_z = 0.5$, for, from left to right, $Ha = 0, 20, 50, 100, 200$; $Pr = 0.71$

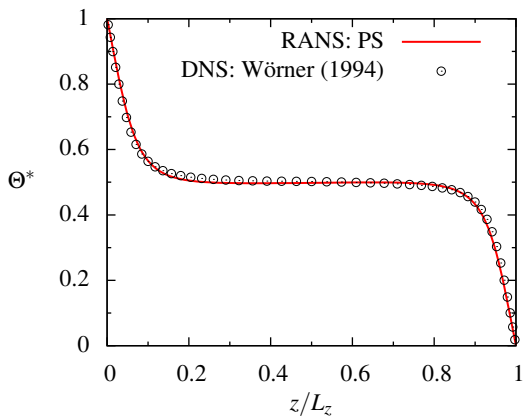


Figure 6. Long-term time averaged vertical temperature profiles in Rayleigh-Bénard convection at $Ra = 6.3 \times 10^5$ and $Pr = 0.71$

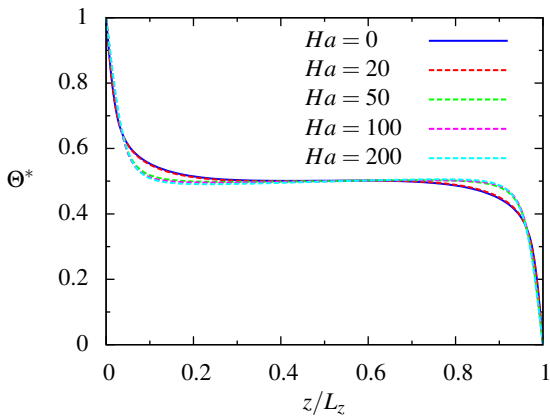


Figure 7. Long-term time averaged vertical temperature profiles for different values of Hartmann number (Ha); $Ra = 10^7$, $Pr = 0.71$

ticeable, deformation of the temperature profile and a reduction in the overall level of the modelled contribution to k when compared with the non-magnetic case. Upon an increase in magnetic field strength to $Ha = 50$, the mean temperature profile undergoes a significant deformation, resulting in an elongation of the uniform core and a thinning of the thermal boundary layer. This deformation continues, although to a much less degree, with further increases in the Hartmann number to $Ha = 100$ and $Ha = 200$. For non-magnetic convection an extension to the uniform core is usually brought about by an increase in Rayleigh number, since the higher level of associated turbulence leads

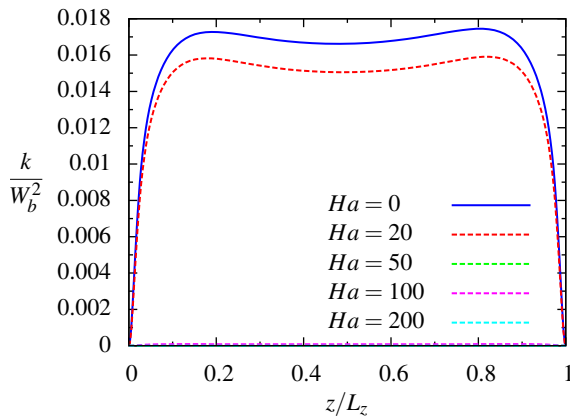


Figure 8. Long-term time averaged profiles of the modelled contribution to the non-dimensional turbulent kinetic energy (with $W_b = \sqrt{g\beta\Delta\Theta L_z}$), for different values of Hartmann number (Ha); $Ra = 10^7$, $Pr = 0.71$

to increased mixing. Profiles of the modelled contribution to the turbulent kinetic energy (Figure 8), however, reveal this has been completely suppressed by the magnetic field by $Ha = 50$.

The qualitative comparisons in Figures 9 and 10 provide an answer to the above contradiction, where considerable changes to the unsteady thermal structures within the flow are seen. For $Ha = 0$ and $Ha = 20$, there are a small number of large plumes, with rounded peaks, which sparsely populate the domain. At $Ha = 50$, the plumes break down into a larger number of thinner plumes, which are more cylindrical in nature, due to a reduction in horizontal mixing. This is in agreement with Hanjalić & Kenjereš (2000), who note that the taller, thinner, plumes facilitate more direct heat transfer between the two walls since the momentum induced by the buoyant force is consumed mainly in the vertical, undamped motion of the plumes. This is also consistent with the findings in the Hartmann flow case, where the magnetic field was seen to reduce the gradients of those quantities not aligned with the magnetic field.

As an extension to the results presented by Hanjalić & Kenjereš (2000), the above trend is seen to continue with a further increase in the magnetic field strength to $Ha = 200$. A curious difference, however, is the prediction here that the thinner plumes tend to arrange in clusters (see Figure 9), in a less orderly fashion than that seen by Hanjalić & Kenjereš (2000). It is worth noting that simulations performed without the KH electromagnetic damping terms (not shown here) did not predict such a significant reduction in turbulence and the accompanied structural reorganisation of the

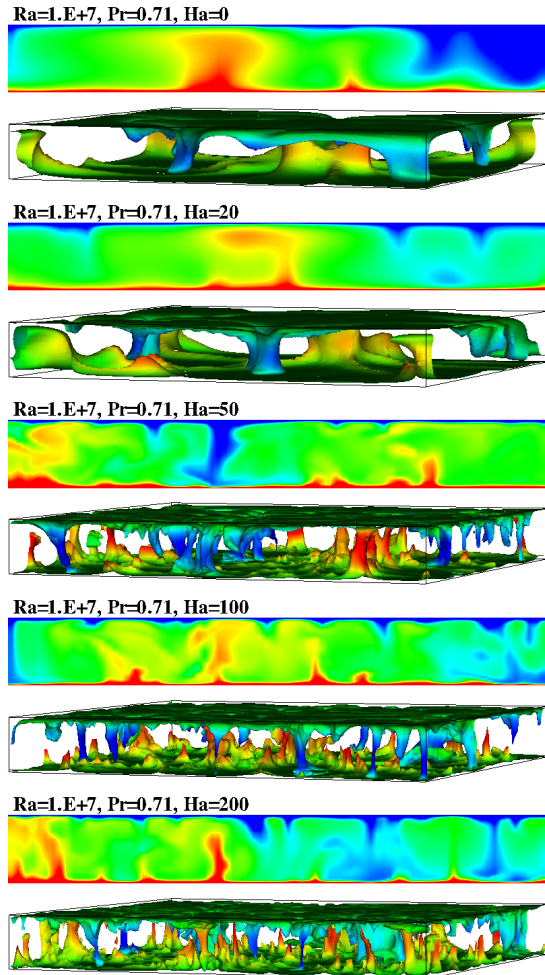


Figure 10. Snapshots showing contours of non-dimensional temperature ($0.3 < \Theta < 0.7$) in the central vertical plane, $y/L_y = 0.5$, and isosurfaces of temperature ($\Theta = 0.35, 0.65$) coloured by the non-dimensional vertical velocity ($-0.3 < W^* = W/\sqrt{g\beta\Delta\Theta L_z} < 0.3$) for, from top to bottom, $Ha = 0, 20, 50, 100, 200$; $Pr = 0.71$

flow.

Low Prandtl Number Cases

We now present results of magnetic Rayleigh-Bénard convection at the lower Prandtl number of $Pr = 0.01$, which is more representative of fluids which typically conduct electricity (i.e. liquid metals). Figure 11 shows the long-term time averaged vertical temperature profiles with increasing magnetic field strength. For non-magnetic convection, the lower Prandtl number facilitates better heat transfer by conduction, which results in much thicker thermal boundary layers than those observed at the higher Prandtl number. With the introduction of the magnetic field at low Hartmann number ($Ha = 20$), the temperature profile shows the reverse of the trend seen at the higher Prandtl number. That is, a small decrease in the extent of the uniform temperature core is observed, with an increase in the thickness of the thermal boundary layers. Then, at a Hartmann number of $Ha = 50$, this trend is reversed, and as the magnetic field strength is increased further the uniform core is again extended into the thermal boundary layers, although in a much more gradual fashion than seen in

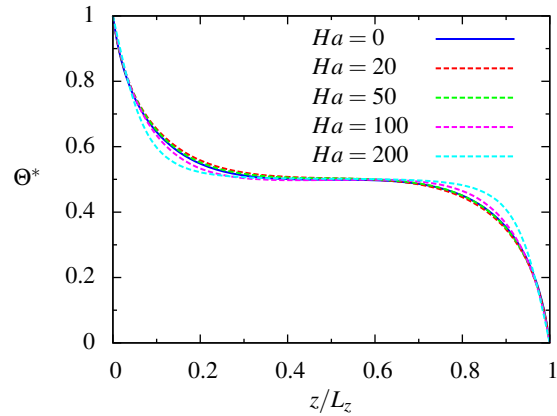


Figure 11. Long-term time averaged vertical temperature profiles for different values of Hartmann number (Ha); $Ra = 10^7$, $Pr = 0.01$

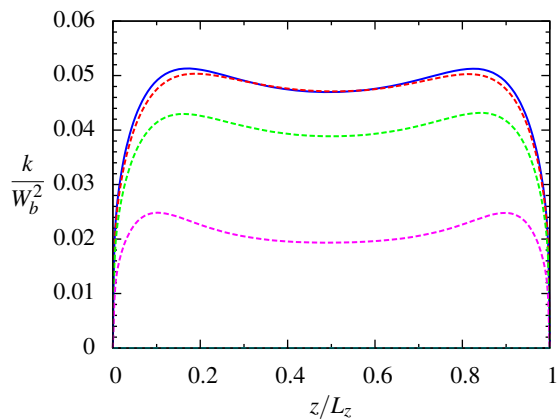


Figure 12. Long-term time averaged profiles of the modelled contribution to the non-dimensional turbulent kinetic energy (with $W_b = \sqrt{g\beta\Delta\Theta L_z}$) for different values of Hartmann number (Ha); $Ra = 10^7$, $Pr = 0.01$

the higher Prandtl number cases.

The profiles of the modelled contribution to the turbulent kinetic energy are shown in Figure 12 where the increased deformation in mean temperature at $Ha > 50$ is accompanied by a gradual reduction in the overall contribution of k to the total turbulent energy. At $Ha = 20$, the magnetic field produces a slight reduction in peak k values and a small increase in the values in the core. The peaks occur at a similar vertical location for both Prandtl numbers, but the thicker thermal boundary layers produced at the low Prandtl number now position the peaks within this boundary layer. At the higher Prandtl number the reduction in mean temperature gradients was only seen once the large reduction in turbulent energy by the magnetic field brought about a significant structural reorganization in the unsteady flow. The structural patterns here, shown in Figures 14 and 13, confirm that this change does not occur until the much higher Hartmann number of around $Ha = 200$, although the changes overall are much more gradual in nature. Hence, without the structural reorganisation which acts to reduce the temperature gradient across the core, the small reduction in k at low Ha serves to decrease overall mixing, leading to the appearance of a thicker boundary layer and more laminar like temperature profile.

August 28 - 30, 2013 Poitiers, France

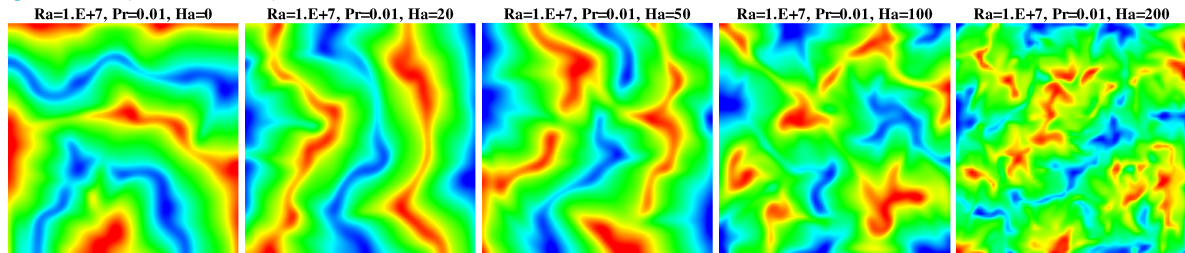


Figure 14. Snapshots showing contours of non-dimensional temperature ($0.15 < \Theta < 0.85$) in the central horizontal plane, $z/L_z = 0.5$, for, from left to right, $Ha = 0, 20, 50, 100, 200$; $Pr = 0.01$

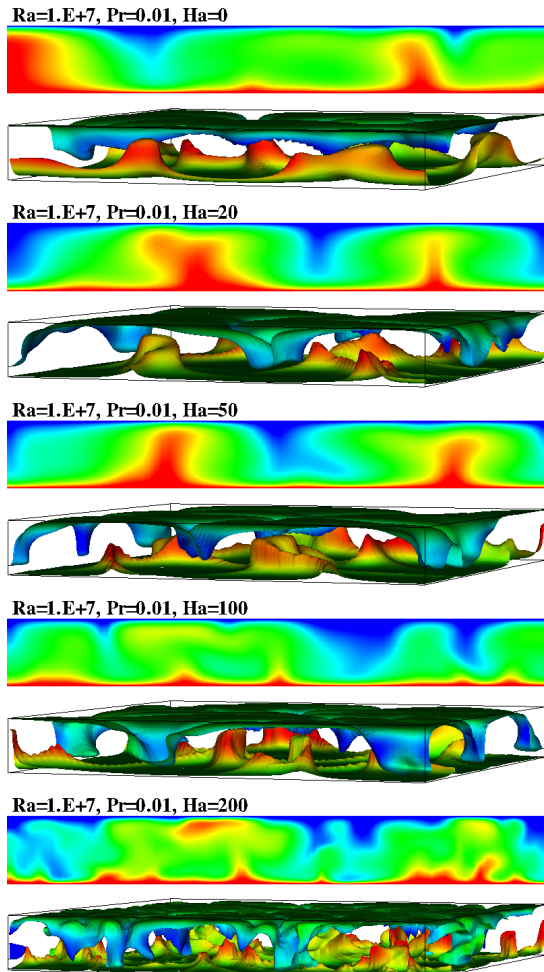


Figure 13. Snapshots showing contours of non-dimensional temperature ($0.15 < \Theta < 0.85$) in the central vertical plane, $y/L_y = 0.5$, and isosurfaces of temperature ($\Theta = 0.2, 0.8$) coloured by the non-dimensional vertical velocity ($-0.3 < W^* = W/\sqrt{g\beta\Delta\Theta L_z} < 0.3$) for, from top to bottom, $Ha = 0, 20, 50, 100, 200$; $Pr = 0.01$

CONCLUSION

The ability of an LEVM to capture the effects of an imposed magnetic field has been investigated through numerical simulations of 2D channel flow and 3D Rayleigh-Bénard convection. In the simple 2D channel flow it was shown that for low values of Ha , both the standard $k-\varepsilon$ and the KH modified version gave good quantitative agreement with DNS data. At higher magnetic fields, however, the KH modifications overpredict the reduction in turbulent

shear stress, believed to be due to an underpredicted modelled magnetic source term in the ε equation. The application of the URANS approach to the simulation of magnetic Rayleigh-Bénard convection over a range of magnetic field strengths ($0 \leq Ha \leq 200$) predicted a significant reorganization of the thermal structures, through both suppression of the turbulent kinetic energy and destruction of gradients in the direction of the magnetic field. For fluid with a moderate Prandtl number, these findings are in agreement with those observed by Hanjalić & Kenjereš (2000). At low Prandtl number, the observed reorganization requires a much higher strength magnetic field. Unfortunately a lack of DNS or experimental data for magnetic Rayleigh-Bénard convection prevents complete validation of these results.

Further modelling work is planned to explore the use of stress transport turbulence models in these flows, where the effect of the magnetic field on the stress anisotropy can, in principle, be better represented.

REFERENCES

- Davidson, P. A. 1999 Magnetohydrodynamics in materials processing. *Annual Review of Fluid Mechanics* **31**, 273–300.
- Hanjalić, K. & Kenjereš, S. 2000 Reorganization of turbulence structure in magnetic Rayleigh-Bénard convection: a t-RANS study. *Journal of Turbulence* **1**, N8.
- Kenjereš, S. & Hanjalić, K. 2000 On the implementation of effects of Lorentz force in turbulence closure models. *International Journal of Heat and Fluid Flow* **21** (3), 329–337.
- Lauder, B. & Sharma, B. 1974 Application of the energy-dissipation model of turbulence to the calculation of flow near a spinning disc. *Letters in Heat and Mass Transfer* **1** (2), 131–137.
- Lien, F. & Leschziner, M. 1994 Upstream monotonic interpolation for scalar transport with application to complex turbulent flows. *International Journal for Numerical Methods in Fluids* **19** (6), 527–548.
- Noguchi, H., Ohtsubo, Y. & Kasagi, N. 2004 DNS database of turbulence and heat transfer. http://www.thtlab.t.u-tokyo.ac.jp/DNS/dns_database.html.
- Satake, Shin-ichi, Kunugi, Tomoaki, Takase, Kazuyuki & Ose, Yasuo 2006 Direct numerical simulation of turbulent channel flow under a uniform magnetic field for large-scale structures at high Reynolds number. *Physics of Fluids* **18** (12), 125106–125106–8.
- Wörner, M. 1994 Direkte simulation turbulenter Rayleigh-Bénard-Konvektion in flüssigem Natrium. Ph.D. thesis, University of Karlsruhe, Kernforschungszentrum Karlsruhe.